INORGANIC CHEMISTRY FRONTIERS

RESEARCH ARTICLE

View Article Online
View Journal | View Issue

Cite this: *Inorg. Chem. Front.*, 2022, **9**, 5169

The modulation mechanism of geometric and electronic structures of bimetallic catalysts: $Pd_{13-m}Ag_m$ (m=0–13) clusters for acetylene semi-hydrogenation†

Panpeng Wei,[a] Jian Zheng,[a] Qiang Li,[b] Yucai Qin,*[b] Huimin Guan,[b] Duping Tan[c] and Lijuan Song *[a,b]

Received 9th June 2022,
Accepted 31st July 2022

DOI: 10.1039/d2qi01222g

rsc.li/frontiers-inorganic

The modulating mechanism of the second metal in bimetallic catalysts for the catalytic properties has always been a hot topic. $Pd_{13-m}Ag_m$ (m=0–13) clusters are used as the model catalysts to explore the influence of Ag-induced configurational and electronic evolution of the PdAg phase on the catalytic performance of acetylene semi-hydrogenation by theoretical calculations. From the results obtained, it can be found that the activity/selectivity to ethylene dramatically depends on the geometric and electronic structures of 13-atom bimetallic clusters in the subnanometer size regime. The adsorption configuration of the C_2 species is determined by the structure of bimetallic clusters, which can be attributed to the reasonable matching with the highest occupied molecular orbital (HOMO). A metastable composition Pd_6Ag_7 cluster, exhibiting the biggest difference in electrons supplied from the clusters to acetylene and ethylene, promotes the reaction path of the target product in the semi-hydrogenation of acetylene. The modulating mechanism of silver has been deeply explored in this paper, which will provide important theoretical guidance for the rational design and development of bimetallic catalysts.

Introduction

Bimetals are high-profile catalytic materials due to their superior catalytic properties which are strongly associated with their intrinsic geometric/electronic structures.[1–3] The exploration of the modulation mechanism opens new perspectives for precise synthetic control of bimetallic active sites.[4–6]

Palladium–silver catalysts have found successful applications in the acetylene semi-hydrogenation industry that requires the conversion of trace amounts of acetylene (~0.1–1%) produced by steam cracking furnaces into ethylene and its reduction to below 1 ppmv.[7–9] Currently, the major issues are the complete hydrogenation of acetylene to ethane and the oligomerization of unsaturated hydrocarbons.[8] Therefore, enhancing the palladium–silver catalyst selectivity to ethylene has been the focus of research on the acetylene semi-hydrogenation process.

The existence of d holes makes the Pd d orbital possess high-energy electrons in consecutive ensembles, which can activate acetylene and ethylene to achieve sp^3 hybridization and result in tetra-σ and di-σ adsorption modes, respectively, favoring complete hydrogenation to ethane.[10–12] The widely accepted strategy is to tune the geometric and electronic structures of the metal active phase of Pd-based catalysts by doping promoter metals to reduce the d-electron energy and break large Pd ensembles.[13–15] Ag alloying of Pd may dilute the Pd atoms, which can inhibit the generation of the non-selective PdH_x phase as the main cause of over-hydrogenation to C_2H_6.[8,16,17] An electron transfer from Ag to Pd, increasing the electron density of the Pd d-band in a bimetallic system, can weaken the adsorption of hydrogen, acetylene, ethylene and other C_2 intermediates on the PdAg catalyst, which is beneficial for improving the ethylene selectivity.[13,18,19] Theoretical study results suggested that Ag atoms tend to be exposed to the surface of a silver-rich system, which is conducive to the formation of isolated Pd atoms.[16,20–22] They also confirmed that Ag donates electrons to Pd, weakening the adsorption strength of related C_2 species on the Pd site, which is consistent with the results of experiments.

For the fabrication of catalysts with adequate activity and stability, the active species of dispersed metal catalysts are often small clusters.[4,23–25] Constructing appropriate spatial

[a]*College of Chemistry and Chemical Engineering, China University of Petroleum, Qingdao, Shandong 266580, China. E-mail: lsong56@263.net*
[b]*Key Laboratory of Petrochemical Catalytic Science and Technology, Liaoning Province, Liaoning Petrochemical University, Fushun, Liaoning 113001, China*
[c]*Lanzhou Petrochemical Research Center, Petrochemical Research Institute, Petrochina, Lanzhou 730060, China*

†Electronic supplementary information (ESI) available. See DOI: https://doi.org/10.1039/d2qi01222g

structures and electronic properties is a long-term goal for the design of metal cluster catalysts.[4,26,27] The dopant of heteroatoms may drastically transform the structural and electronic properties of the bimetallic phase because of the different nucleation and growth modes of metals, which was also confirmed by our previous study.[28–30] However, limited by the analysis tools available, few research studies have been able to achieve sensitivity of the catalytic performance to the second metal-induced spatially geometric and electronic structures of bimetallic species in the subnanometer size regime. This is still unclear despite it being crucial for optimizing the catalytic performance of bimetallic catalysts.

PdAg clusters can be used as high-performance and cost-effective catalytic materials for acetylene semi-hydrogenation.[31,32] The change of just one atom in clusters may cause a variation of the ensembled morphologies, local coordination environments, electronic properties and so on.[26,33] The evolution of the structure (geometric/electronic) may affect the chemisorption configurations of relevant molecules, which play an important role in the catalysis.[9,10] For acetylene hydrogenation, a catalyst with specific well-defined geometric and electronic structures is expected to efficiently adjust and catalyze the rate-determining step (RDS) and provide excellent reactivity to ethylene.[34] One of the challenges is that the similar atomic scattering factors of Pd and Ag cause the experimental studies to provide ensemble-average information and to be unable to identify the crucial active metal component favoring the conversion of acetylene to ethylene.[19,35] The explicit structural and electronic information correlates with catalytic properties can be provided by density functional theory (DFT) calculations.

In the present work, we carried out DFT calculations combined with Monte Carlo simulation to systematically investigate the modulating mechanism of silver on the activity/selectivity of acetylene semi-hydrogenation over $Pd_{13-m}Ag_m$ (m=0–13) clusters. This is pivotal to disentangling the modulation mechanism of the second metal in bimetallic catalysts, and it has allowed us to comprehend in-depth the effect of Ag-induced configurational evolution and the resulting electronic structure of bimetallic clusters on the activity and selectivity in harsh reaction conditions. The RDS of acetylene hydrogenation varies with the evolution of the cluster structure. With these central insights, we notice that a metastable Pd_6Ag_7 cluster having a unique geometric and electronic structure seems to exhibit extraordinary acetylene hydrogenation activity and poor ethylene adsorption capacity, showing optimal activity and selectivity.

Computational details

The calculations were carried out with the density-functional theory (DFT) method, as performed using the Cambridge Serial Total Energy Package (CASTEP) plane-wave code in the Materials Studio 5.5 software package, Accelyrs.[36] The generalized gradient approximation (GGA) and the Perdew-Wang 91 generalized gradient approximation (GGA-PW91) functional were selected and used the formal spin as initial (the initial value for the number of unpaired electrons for each atom will be taken from the formal spin specified for each atom and subsequently optimized during the calculation) to calculate the character of the base state.[37] The available 13-atom palladium–silver clusters and the corresponding pure cluster structures mentioned in our previous work were used for the growth method considering simulated annealing.[29] All calculations were performed in a 15 Å cubic lattice with a Gamma k-point and a cutoff energy of 450 eV. The force threshold and self-consistent tolerance were set to 0.03 eV $Å^{-1}$ and 10^{-6} eV per atom, respectively. Double numerical plus polarization (DNP) was employed with a smearing of 0.05 eV. The parameters in our calculations were carefully tested, with the change of the calculated energy being smaller than 2%. A complete LST (linear synchronous transit)/QST (quadratic synchronous transit) method was used to search for the transition state (TS) of every elementary reaction and all transition states had only one imaginary frequency.

The adsorption free energy (ΔG_{ads}) of adsorbates on clusters, the activation free energy (G_a) and the reaction free energy (ΔG) were calculated using

$$\Delta G_{ads} = E_{Ads/Cluster} + G_{Ads/Cluster} - (E_{Ads} + G_{ads} + E_{Cluster} + G_{Cluster}) \quad (1)$$

$$G_a = E_{TS} + G_{TS} - (E_R + G_R) \quad (2)$$

$$\Delta G = E_P + G_P - (E_R + G_R) \quad (3)$$

where $E_{Ads/Cluster}$, E_{Ads}, $E_{Cluster}$, E_{TS}, E_R and E_P are the energy of clusters with adsorbates, gas-phase adsorbates, bare clusters, transition states, reactants and products, respectively. $G_{Ads/Cluster}$, G_{Ads}, $G_{Cluster}$, G_{TS}, G_R and G_P are the corresponding standard free energies at a finite temperature.

The d-band center (ε_d) is defined as the following:[38,39]

$$\varepsilon_d = \frac{\int \varepsilon \Delta\varepsilon d_\varepsilon}{\int \Delta\varepsilon d_\varepsilon} \quad (4)$$

where ε and $\Delta\varepsilon$ are the DOS and weighted DOS, respectively.

Results and discussion

Structural evolution of $Pd_{13-m}Ag_m$–C_2H_x (x=2, 4) systems

The multiple low-energy adsorption sites of acetylene on $Pd_{13-m}Ag_m$ (m = 0–13) clusters were found using Adsorption Locator (based on Monte Carlo simulation with the CAMPASS force field) with 10 cycles and 100 000 steps per cycle;[40,41] only the most favorable adsorption configurations with the lowest energy are presented in Fig. 1. For acetylene adsorption on the Pd-based catalyst, four adsorption modes are proposed: tetra-σ mode, with each carbon atom of acetylene binding to two substrate atoms respectively; di-σ mode, with two carbon atoms of acetylene binding to two substrate atoms; π mode, with two carbon ends of acetylene binding to one substrate atom; and

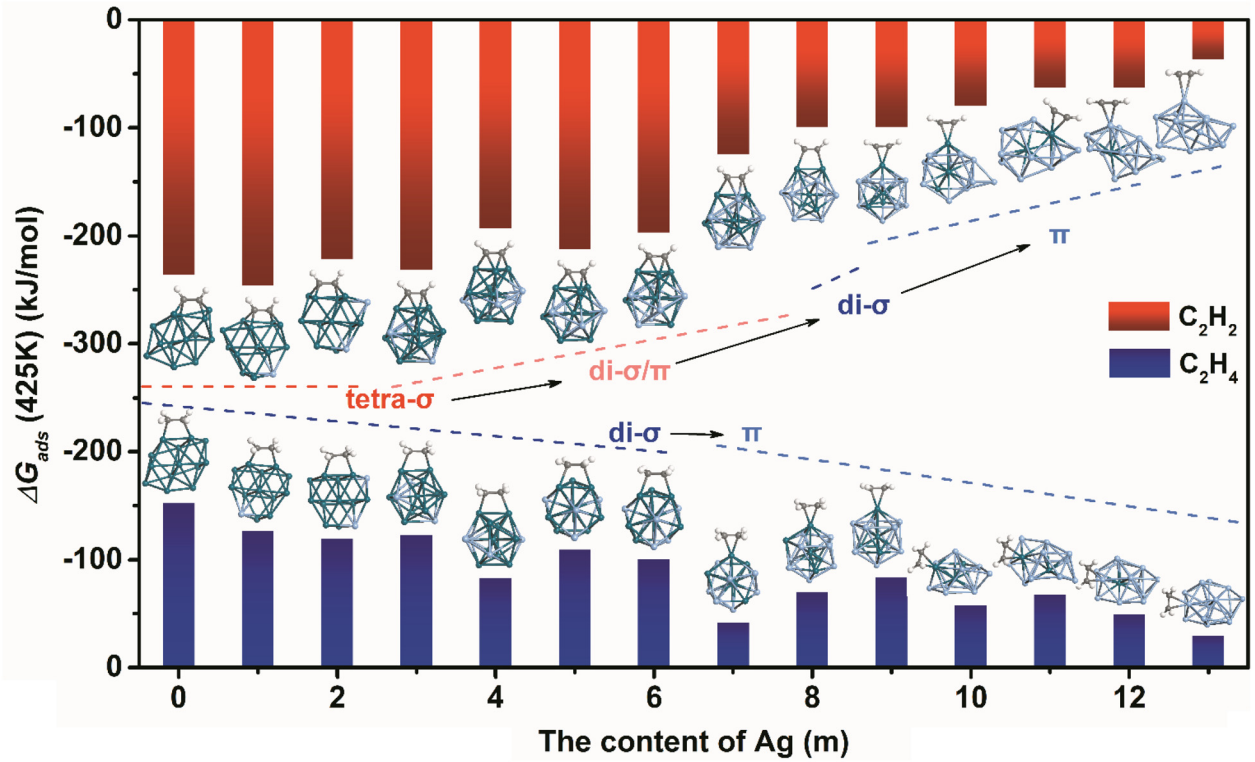

Fig. 1 The most stable adsorption configurations, adsorption free energies (ΔG_{ads}, kJ mol^{-1}, 425 K) and adsorption modes of $Pd_{13-m}Ag_m$–C_2H_x (top, C_2H_2; and bottom, C_2H_4). Dark green, Pd; light blue, Ag; gray, C; and white, H.

di-σ/π mode, with two carbon ends of acetylene not only binding to two substrate atoms, but also jointly binding to the third substrate atom (*via* two σ-bonds and one π-bond).[9,10,22,42,43]

The contributions of various translations, vibrations and rotations of the systems are reflected by G (T). The adsorption free energies (ΔG_{ads}) of C_2H_2 and C_2H_4 at 425 K were calculated,[44] as shown in Table 1. Acetylene preferentially adsorbs on the Pd_{13} cluster in the tetra-σ mode, yielding an adsorption free energy of −264.70 kJ mol^{-1} (Fig. 1 and Table 1). The adsorbed C_2H_2 is activated and the C–C bond is stretched from 1.21 (gas phase) to 1.39 Å. The adsorption mode of acetylene on $Pd_{12}Ag$ is similar to that on Pd_{13}. The ΔG_{ads}, −246.07 kJ mol^{-1}, is larger than that of Pd_{13}, but the deformation of C_2H_2 and the $Pd_{12}Ag$ cluster is more serious because of the evolution of the cluster configuration caused by

Table 1 Adsorption modes, adsorption free energies (ΔG_{ads}, 425 K, kJ mol^{-1}) and carbon–carbon bond distances (d_{C-C}) of C_2H_2 and C_2H_4 and the d-band center of $Pd_{13-m}Ag_m$ (m = 0–13) clusters

	Mode			ΔG_{ads} (kJ mol^{-1})		d_{C-C}[a] (Å)	
M (Ag atom)	C_2H_2	C_2H_4	ε_d (eV)	C_2H_2	C_2H_4	C_2H_2	C_2H_4
0	Tetra-σ	Di-σ	−1.96	−264.70	−152.36	1.39	1.43
1	Tetra-σ	Di-σ	−2.04	−246.07	−126.09	1.40	1.42
2	Tetra-σ	Di-σ	−2.09	−221.30	−119.16	1.40	1.43
3	Di-σ/π	Di-σ	−2.14	−231.80	−122.39	1.35	1.44
4	Di-σ/π	Di-σ	−2.23	−193.70	−82.87	1.35	1.44
5	Di-σ/π	Di-σ	−2.29	−212.40	−108.95	1.34	1.44
6	Di-σ/π	Di-σ	−2.46	−197.00	−100.12	1.35	1.43
7	Di-σ/π	π	−2.52	−124.31	−41.64	1.32	1.39
8	Di-σ	π	−2.63	−99.05	−69.54	1.29	1.39
9	π	π	−3.53	−99.16	−83.29	1.26	1.39
10	π	π	−2.99	−79.49	−57.44	1.25	1.39
11	π	π	−3.52	−62.65	−67.67	1.25	1.38
12	π	π	−3.44	−63.04	−49.31	1.22	1.36
13	π	π	−3.96	−36.70	−29.66	1.22	1.36

[a] The calculated values of d_{C-C} of gas-phase C_2H_2, C_2H_4 and C_2H_6 in the gas phase are 1.21, 1.33, and 1.53 Å, respectively.

the doping of Ag atoms (Table S1†). Acetylene adsorption on the $Pd_{11}Ag_2$ cluster *via* the tetra-σ-bound mode is close to that on $Pd_{12}Ag$ that has a ΔG_{ads} of −221.30 kJ mol^{-1}.

Acetylene adsorption on $Pd_{10}Ag_3$ is the di-σ/π mode, yielding a ΔG_{ads} of −231.80 kJ mol^{-1}, suggesting that with the increase of doped Ag atoms, the adsorption configuration of acetylene transforms with the evolution of the cluster structure and the adsorption strength decreases. For Pd_9Ag_4, acetylene adsorption prefers the di-σ/π-bound state, which accounts for a ΔG_{ads} of −193.70 kJ mol^{-1}. Interestingly, in the geometry optimization of acetylene adsorption on the Pd_8Ag_5 cluster, the adsorption mode is the same as that of Pd_9Ag_4, but the adsorption free energy is −212.40 kJ mol^{-1}, being lower than that of Pd_9Ag_4. This may be attributed to the difference in cluster structures, that is, the Ag-induced structural evolutions affect the adsorption of acetylene.

Acetylene interacts with the Pd_6Ag_7 cluster *via* σ-bonding to two Pd atoms and an unusual π-mode interaction with an Ag atom; the most favorable adsorption configuration is shown in Fig. 1. The corresponding adsorption free energy is −124.31 kJ mol^{-1}. With the increase of Ag atom content from 7 to 8 in the bimetallic cluster, the most favorable adsorption configuration of acetylene is the di-σ state rather than the di-σ/π mode with a ΔG_{ads} of −99.05 kJ mol^{-1}. The energetically preferred adsorption configurations of acetylene on $Pd_4Ag_9 \sim Ag_{13}$ clusters are shown in Fig. 1, *via* the π-bound mode. The calculations yield values of ΔG_{ads} of −99.16 kJ mol^{-1} (Pd_4Ag_9), −79.49 kJ mol^{-1} (Pd_3Ag_{10}), −62.65 kJ mol^{-1} (Pd_2Ag_{11}), −63.04 kJ mol^{-1} ($PdAg_{12}$) and −36.70 kJ mol^{-1} (Ag_{13}).

Our results show that the low-energy adsorption configurations of ethylene on $Pd_{13-m}Ag_m$ clusters only two modes are presented: di-σ mode and π mode, in line with what has been reported.[9,10,20,45] The most stable adsorption configuration of ethylene on the Pd_{13} cluster *via* the di-σ-bound mode is presented in Fig. 1. This di-σ structure yields a ΔG_{ads} of −152.36 kJ mol^{-1}, which is 112.34 kJ mol^{-1} higher than that of acetylene adsorption (Table 1). Ethylene adsorption on $Pd_{12}Ag \sim Pd_9Ag_4$ clusters also *via* the di-σ-bound mode is shown in Fig. 1. These di-σ structures yield values of ΔG_{ads} of −126.09 kJ mol^{-1} ($Pd_{12}Ag$), −119.16 kJ mol^{-1} ($Pd_{11}Ag_2$), −122.39 kJ mol^{-1} ($Pd_{10}Ag_3$) and −82.87 kJ mol^{-1} (Pd_9Ag_4), which increase with the increase of Ag atom content. For ethylene adsorption on Pd_8Ag_5 (−108.95 kJ mol^{-1}), the calculations found identical di-σ-bound state energy minimum structures but it was more stable than Pd_9Ag_4. Geometry optimization of ethylene adsorption on the Pd_7Ag_6 cluster yielded the di-σ-bound mode with a ΔG_{ads} of −100.12 kJ mol^{-1}.

Ethylene adsorption on both Pd_6Ag_7 and Pd_5Ag_8 prefers the π-bound state, which separately accounts for values of ΔG_{ads} of −41.64 and −68.54 kJ mol^{-1}. The Pd_4Ag_9 cluster has an anomaly with a ΔG_{ads} of −83.29 kJ mol^{-1}, which is 13.78 kJ mol^{-1} lower than the ethylene adsorption on Pd_5Ag_8 with a similar adsorption mode (Fig. 1 and Table 1). For ethylene adsorption on $Pd_3Ag_{10} \sim Ag_{13}$ clusters, the adsorption modes are all the π-bound state, possessing values of ΔG_{ads} of −57.44, −67.67, −49.31 and −29.66 kJ mol^{-1}, respectively.

To interpret the adsorption behaviors in more detail, ΔE_{ads} is divided into three contributions according to $\Delta E_{ads} = E_{def}(C_2H_x) + E_{def}(Pd_{13-m}Ag_m) + E_{int}$. According to the data summarized in Table S1,† we can see that the acetylene deformation energies (E_{def}) for the tetra-σ, di-σ/π, di-σ and π structures are within the ranges of 258.99–274.54, 172.66–200.66, 129.57 and 3.49–46.11 kJ mol^{-1}, respectively. The E_{def} of acetylene increases with the extension of the C–C bond activated by the clusters (Tables 1 and S1†). The tetra-σ-bound mode always induces a greater extension (with regard to the gas phase) than the others in our studies. The C–C bond distance (d_{C-C}) in the tetra-σ, di-σ/π, di-σ and π modes enlarged to ∼1.40, 1.34, 1.29 and 1.24 Å from 1.21 Å in the gas phase, while the π-bound structures of acetylene on $PdAg_{12}$ and Ag_{13} show only a slight and almost negligible elongation (∼1.22 Å).

Further analysis shows that the ethylene deformation energies for the di-σ and π structures are within the energy ranges of 71.99–89.99 and 4.19–22.94 kJ mol^{-1}, respectively. The E_{def} of ethylene increases with the extension of the C–C bond too. The di-σ structures always induced a greater extension than the π modes compared with the gas phase. The d_{C-C} in the di-σ-bound mode enlarged to ∼1.43 Å from 1.33 Å (gas-phase), while the π-bound structures caused a smaller C–C bond elongation (∼1.38 Å).

An in-depth study of E_{def} shows that the deformation of adsorbates is much stronger than that of the adsorbents. As the largest deformation energies of the adsorbed acetylene and ethylene are 274.54 and 89.99 kJ mol^{-1}, the deformation energies of $Pd_{13-m}Ag_m$ clusters are rather small, below 53.30 and 15.99 kJ mol^{-1}, respectively. The energy consumption for the deformation can be compensated for by the interaction between the adsorbates and the clusters. Despite the $Pd_{13-m}Ag_m$–C_2H_x interaction in various modes, E_{int} could compensate for the energy cost of deformation between the adsorbates and the bimetallic clusters.

It can be seen that the interaction between clusters and C_2H_x is affected not only by the content of Ag around Pd, but also the geometric structure of $Pd_{13-m}Ag_m$ clusters is a factor that cannot be underestimated. Our calculation shows that the ΔG_{ads} (425 K) of C_2H_2 adsorption is always greater than that of C_2H_4 on the 13-atom bimetallic clusters (except for Pd_2Ag_{11}). Meanwhile, for C_2H_x adsorption on Pd_2Ag_{11}, $PdAg_{12}$ and Ag_{13} clusters, there are small differences in the values of ΔG_{ads} (425 K) between the two adsorbates (Fig. 1). In summary, the stability of acetylene adsorption on the $Pd_{13-m}Ag_m$ clusters is better than that of ethylene, excluding Pd_2Ag_{11} at 425 K. However, the acetylene semi-hydrogenation process is used to remove trace (∼0.1–1%) acetylene in ethylene, so $m \geq 11$ is not conducive.

Electron interaction in $Pd_{13-m}Ag_m$–C_2H_x systems

The partial densities of states (PDOSs) for $Pd_{13-m}Ag_m$ clusters before and after C_2H_x adsorption are shown in Fig. 2 and S1–S7.† In general, the adsorption stability is mainly determined by the bond strength of adsorbed molecules, increasing in the order tetra-σ > di-σ/π > di-σ > π (for acetylene) and di-σ > π (for

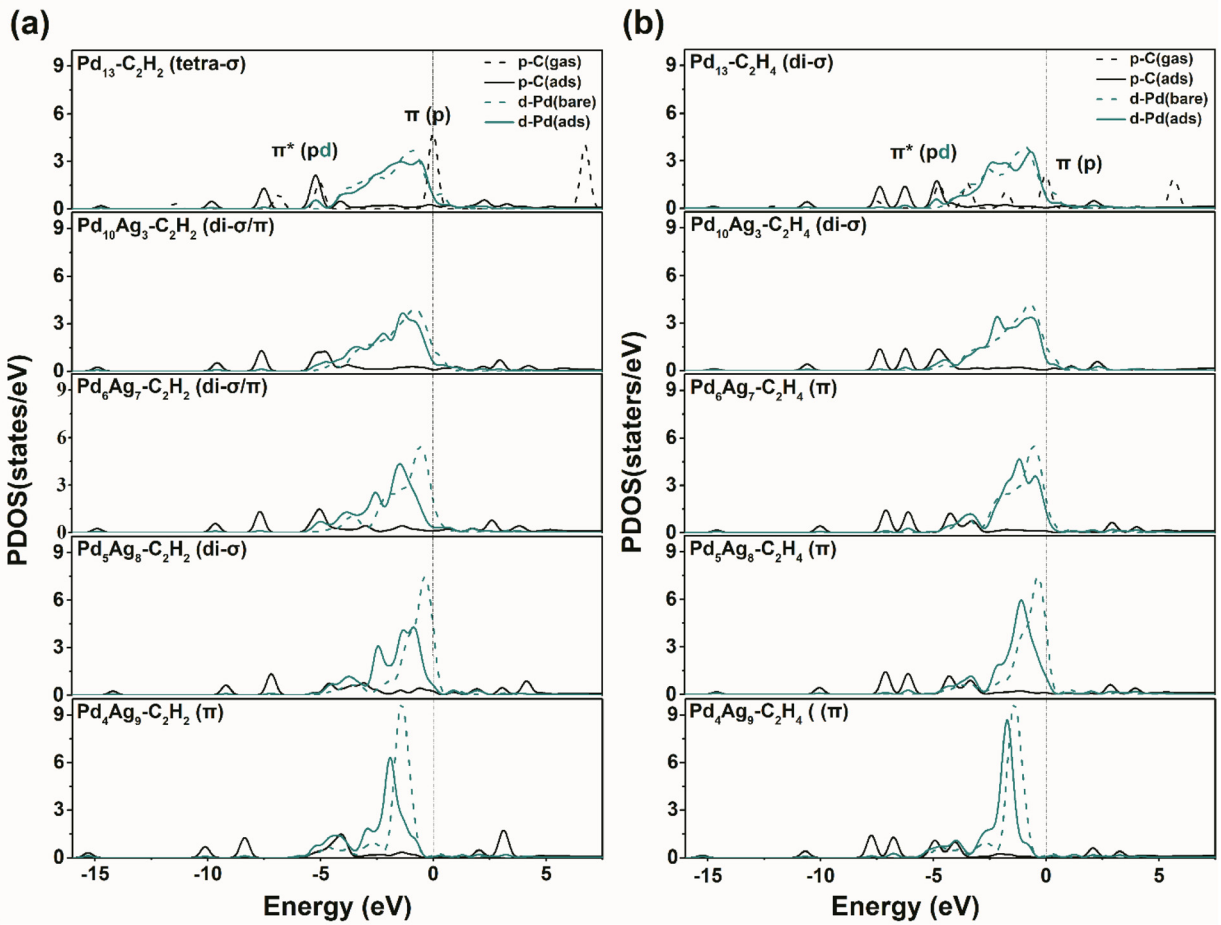

Fig. 2 Partial densities of states (PDOSs) for Pd_{13}, $Pd_{10}Ag_3$, Pd_6Ag_7, Pd_5Ag_8 and Pd_4Ag_9 clusters (different adsorption modes) projected on the bonded Pd atoms and C atoms in acetylene (a) and ethylene (b) before and after adsorption. Dotted lines, before adsorption, and solid lines, after adsorption.

ethylene) (Fig. 1). For C_2H_x adsorption, the *d* band states of Pd resonate with the *p* band states of carbon in $Pd_{13-m}Ag_m$–C_2H_x systems, forming the π^*_{pd} orbital. The *p* orbitals of carbon atoms strongly mixed with the low-energy (typically below the Fermi level) *d* states of Pd atoms, while for the *d* states, the distribution is wider and more delocalized but still localize at the metal cluster. The *d* states of Pd show a finite density of states at the Fermi level.

The *p* states of carbon from acetylene are more delocalized than those of carbon from ethylene, indicating that the interactions between acetylene and $Pd_{13-m}Ag_m$ are stronger. There are also significant differences in the resonances of *p* states near the Fermi level, and that of *p* states of carbon in acetylene is stronger. We note that both the *d*-band state of Pd and the *p* states of C are moving towards the lower energy region after C_2H_x adsorption, compared with the bare clusters and C_2H_x. This means that the adsorption of C_2H_x induces charge redistribution. The *d*-band center can be used as a "descriptor" to describe the adsorption of the adsorbent.[38,39,46] As shown in Table 1, an electron transfer from Ag to Pd effectively reduces the *d*-band center of $Pd_{13-m}Ag_m$, possibly weakening the adsorption of Pd on hydrogen and related C_2 hydrocarbon, which inhibits over-hydrogenation.

The variation of electronic density spatial distribution (electronic density difference) is shown in Fig. 3 and S9.† The positive (green) and negative (yellow) areas indicate where the electron density is enriched or depleted, respectively. C_2H_x are adsorbed on $Pd_{13-m}Ag_m$ and an electron transfer apparently occurs in the $Pd_{13-m}Ag_m$–C_2H_x systems. Electronic interactions between C_2H_x and the bimetallic clusters with the tetra-σ mode are the strongest and the weakest are π-interactions. The carbon atoms in C_2H_x obtain electrons from the clusters through the Pd/Ag atoms bonded to them. The Pd/Ag atoms lose electrons in d_{z^2}-like orbitals, which is associated with the charge redistribution of the formed C–Pd/C–Ag bonds. At the same time, the bonded metal atoms also obtain electrons from other Pd/Ag atoms in the clusters to compensate for the loss. The increase of electronic density (the green areas) is embodied on C_2H_x with a π*-like distribution, and in d_{xz} and d_{yz} combinations on Pd atoms. As an increase in the content of Ag atoms in the clusters leads to the evolution of adsorption configuration, the electrons contributed by the cluster to C_2H_x

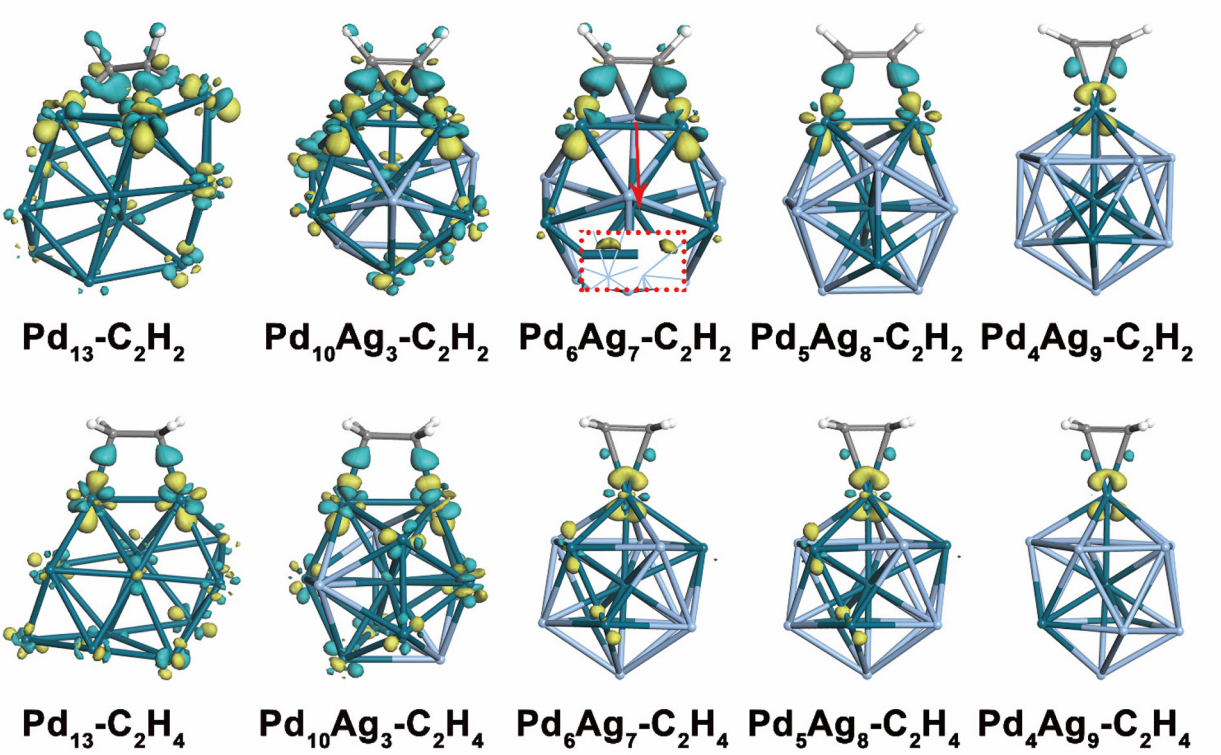

Fig. 3 Electron density difference for acetylene (upper) and ethylene (bottom) adsorbed on Pd_{13}, $Pd_{10}Ag_3$, Pd_6Ag_7, Pd_5Ag_8 and Pd_4Ag_9 clusters. The green and yellow areas indicate where the electron density is enriched or depleted; the color scheme is identical to that in Fig. 1.

decrease. Thus, the interactions between bimetallic clusters and C_2H_x weaken. The interaction of C_2H_2 with the Ag in Pd_6Ag_7 is also evidenced by Ag donating electrons to C and the overlap of the orbital from the PDOS (see Fig. 3 and S8†).

In the $Pd_{13-m}Ag_m$–C_2H_x systems, Ag transfers electrons to Pd, which in turn transfers electrons to C atoms, following the order of electronegativity: C > Pd > Ag. The Hirshfeld charge of Pd atoms interacting with C_2H_x was analyzed, aiming at further clarifying the effect of electron interaction on the adsorption behavior of C_2H_x over $Pd_{13-m}Ag_m$ clusters (Fig. 4). Among the $Pd_{13-m}Ag_m$, the discrepancy between the electron lost by Pd after acetylene adsorption and that lost after ethylene adsorption is the largest in Pd_6Ag_7, which may be beneficial for the removal of trace acetylene in ethylene.

The frontier molecular orbital analysis was performed according to the differential charge density result, from which the lowest unoccupied molecular orbital (LUMO) of C_2H_x and the highest occupied molecular orbital (HOMO) of $Pd_{13-m}Ag_m$ clusters are obtained (see Fig. 5 and S10†). The doping of Ag atoms causes the evolution of the HOMO structure of the bimetallic clusters, whose principle is the transformation of metal–metal interaction. To achieve the maximum orbital overlap, the LUMOs of acetylene and ethylene are matched with the HOMOs of $Pd_{13-m}Ag_m$ clusters to form different adsorption configurations.

In particular, the π^*_p-shaped LUMO of acetylene, formed by the *p* orbitals of two carbon atoms, interacts with the HOMO

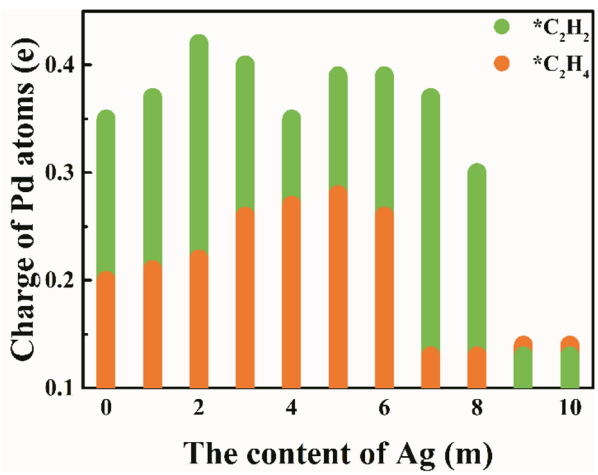

Fig. 4 The Hirshfeld charge of the bonded Pd atoms in $Pd_{13-m}Ag_m$–C_2H_x (m = 0–10) systems.

of Pd_6Ag_7 (two Pd atoms with d_{xz}-shaped orbitals) to form the π^*_{pd} molecular orbital, as shown in Fig. 5. The acetylene molecule (with an *sp* hybrid orbital) rotates to maximize the overlap with the d_{xz}-shaped HOMO orbitals (inclined to the corresponding Pd–Pd–Ag plane, view A in Fig. 5), forming two σ chemical bonds (C–Pd) that are inclined to the corresponding plane. This results in the acetylene molecule approaching the

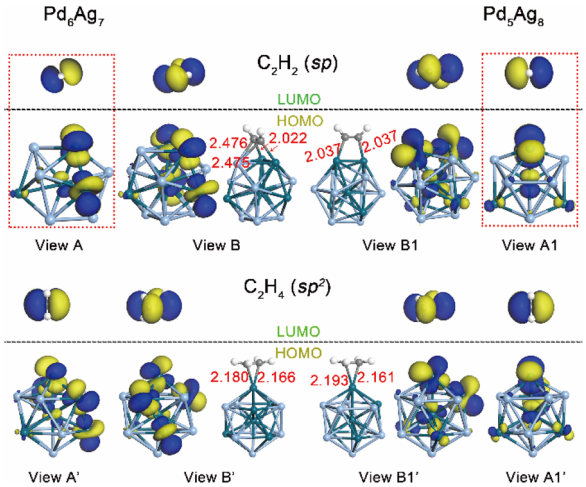

Fig. 5 The lowest unoccupied molecular orbitals (LUMOs) of acetylene and ethylene molecules and the highest occupied molecular orbitals (HOMOs) of Pd_6Ag_7 and Pd_5Ag_8 clusters (the red numbers indicate the bond length, Å). The color scheme is identical to that in Fig. 1.

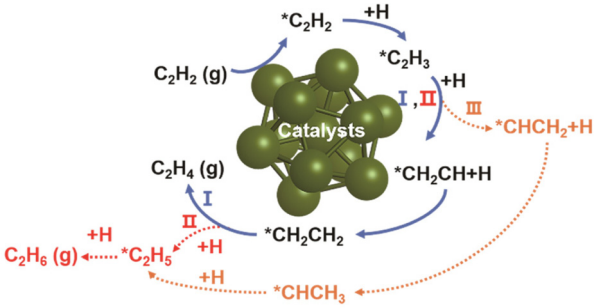

Scheme 1 Possible reaction pathways of C_2H_2 hydrogenation. * The adsorption state and (g) the gas-phase state, respectively.

corresponding Ag atom and interacting with the Ag atom with the π-mode, forming the di-σ/π mode adsorption configuration on the Pd_6Ag_7 cluster. For the ethylene molecule, with an sp^2 hybrid orbital, it can only interact with one d_{xz}-shaped orbital to form the π-mode adsorption configuration. In addition, the two d_{xz}-shaped orbitals, forming bonds with acetylene, have exactly the same interaction with the two carbon atoms, so the lengths of the two C–Pd bonds in the Pd_6Ag_7–C_2H_2 system are also the same (both are 2.022 Å, Fig. 5). However, due to the metal–metal interaction in the cluster, the d_{xz}-shaped orbital loses its original centrosymmetric type, so the interaction with the two carbon atoms in ethylene is different and the C–Pd bond formed is also different, which are 2.180 and 2.166 Å, respectively.

The HOMO of Pd_5Ag_8 is also a d_{xz}-shaped orbital, just suitable for acetylene to bind in a configuration where the C–C bond is directly above the corresponding Pd–Pd bond to achieve the maximum orbital overlap (view A1 in Fig. 5). Therefore, acetylene preferentially adsorbs on the Pd_5Ag_8 cluster in the di-σ mode with the same C–Pd bonds, while ethylene has a π mode adsorption configuration with different C–Pd bonds. From the above analysis, it can be seen that the intra-cluster metal–metal interaction changes the HOMO of the clusters, thereby transforming the adsorption configuration of acetylene and ethylene.

Acetylene hydrogenation process on $Pd_{13-m}Ag_m$

There are three possible reaction paths for acetylene hydrogenation, as shown in Scheme 1; one is acetylene gradually hydrogenated to ethylene and desorbed from the catalyst to form a gas [CH_2CH_2 (g)] and the second and third correspond to the hydrogenation of adsorbed ethylene [CH_2CH_2 (ad)] and ethylidene ($CHCH_3$) to C_2H_5 (ad), respectively, indicating the occurrence of over-hydrogenation.[10,11,47] Therefore, in order to improve the selectivity of ethylene, the latter two paths should be inhibited.

Ag is doped with the Pd cluster, aiming at regulating the reaction path of acetylene hydrogenation along path I. According to this, there are two key steps in the hydrogenation of acetylene on the catalysts, which are the hydrogenation of C_2H_3 species to $CHCH_3$ or CH_2CH_2 (ad) and the generated CH_2CH_2 (ad) preferring desorption or further hydrogenation. First, the activation free energy (G_a) of generating CH_2CH_2 (ad) and $CHCH_3$ from C_2H_3 is differentiated, judging whether the path associated with CH_2CH_2 (ad) is superior to $CHCH_3$. Subsequently, the free energy differences between CH_2CH_2 (ad) desorption and its hydrogenation should be distinguished, which elaborates whether CH_2CH_2 (ad) prefers desorption rather than further hydrogenation (as mentioned above, Pd_2Ag_{11}, $PdAg_{12}$ and Ag_{13} clusters are not considered).

For $m \leq 2$, the activation free energy of C_2H_2 hydrogenation to C_2H_3 increased with the increase of Ag incorporation (Table 2). Pd_{13}, $Pd_{12}Ag$ and $Pd_{11}Ag_2$ contribute the activation free energies of 11.98, 77.25 and 104.29 kJ mol^{-1}, respectively. G_a decreases slightly, 94.99 kJ mol^{-1} for $Pd_{10}Ag_3$, which is assumed to be due to the structural evolution of the bimetallic cluster (from a hexagonal bi-layer to a distorted icosahedral structure). Subsequently, it still shows a downward trend (51.51 kJ mol^{-1} for Pd_9Ag_4). When the content of Ag atoms in $Pd_{13-m}Ag_m$ clusters further increases to m=5, the G_a (C_2H_2 + H) gradually decreases (20.76 kJ mol^{-1} for Pd_8Ag_5), and then it increases again (100.31 kJ mol^{-1} for Pd_3Ag_{10}). That is to say, doping an appropriate amount of Ag in the clusters makes the interaction of $Pd_{13-m}Ag_m$–C_2H_2 moderate and conducive to the reaction. By the way, the geometric structure of the bimetallic clusters is also an important factor.

Doping Ag atoms significantly changes the hydrogenation path of acetylene on the clusters (Fig. 6 and Fig. S11 and S12†). For the co-adsorption configuration of the H atom and the C_2H_3 species on Pd_{13}, the hydrogen atom near the carbon atom bonded with two H atoms in C_2H_3[($CHCH_2$ + H)*] (where * denotes the adsorption state) is superior to the hydrogen atom near the carbon atom bonded with one H atom [(CH_2CH + H)*], and the values of G_a of $CHCH_2$ + H and CH_2CH + H are 20.64 and 157.31 kJ mol^{-1}, respectively. Namely, C_2H_2 prefers

Table 2 The activation free energy (G_a, kJ mol^{-1}) of acetylene hydrogenation related steps, adsorption free energies (G_{co-ads}, kJ mol^{-1}) of acetylene and ethylene co-adsorption with the H atom, ethylene selectivity ΔG_{sel} (kJ mol^{-1}) and the reaction rate of ethylene formation (r per s site) on $Pd_{13-m}Ag_m$ (m = 0–10) clusters at 425 K

	G_a (kJ mol^{-1})				G_{co-ads} (kJ mol^{-1})			
Clusters	$C_2H_2 + H \rightarrow CHCH_2$	$CH_2CH + H \rightarrow CH_2CH_2$	$CHCH_2 + H \rightarrow CHCH_3$	$CH_2CH_2 + H \rightarrow CH_2CH_3$	C_2H_2	C_2H_4	ΔG_{sel} (kJ mol^{-1})	r (per s per site)
Pd_{13}	11.98	157.31	20.64	30.23	−184.49	−108.00	−77.77	0.46
$Pd_{12}Ag$	77.25	145.32	32.72	123.71	−179.02	−119.28	4.43	1.90×10^{-2}
$Pd_{11}Ag_2$	104.29	77.33	4.29	19.06	−220.66	−88.03	−68.97	1.32×10^{2}
$Pd_{10}Ag_3$	94.99	63.26	67.14	101.28	−226.39	−104.48	−3.20	1.25
Pd_9Ag_4	51.51	61.21	88.01	54.78	−204.12	−102.94	−48.16	1.94
Pd_8Ag_5	20.76	52.69	25.53	80.91	−236.90	−85.15	−4.24	2.99×10^{2}
Pd_7Ag_6	29.05	59.62	125.25	44.96	−186.75	−84.27	−39.31	3.83×10^{2}
Pd_6Ag_7	65.59	21.02	—	46.06	−119.15	−23.18	22.88	1.25×10^{10}
Pd_5Ag_8	47.30	52.47	—	49.16	−127.94	−74.98	−25.82	5.32×10^{3}
Pd_4Ag_9	66.41	13.45	—	80.65	−67.21	−60.59	20.06	3.13×10^{5}
Pd_3Ag_{10}	100.31	46.86	—	52.85	−102.61	−59.31	−6.46	4.50×10^{5}

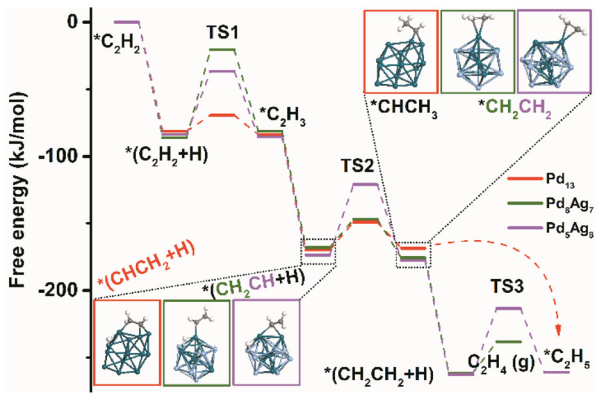

Fig. 6 Potential energy diagram for preferred pathways and the rate-determining step (RDS) involving in acetylene hydrogenation on Pd_{13}, Pd_6Ag_7 and Pd_5Ag_8 clusters (paths I, II and III, respectively) at 425 K (* denotes the adsorption site).

the $CHCH_3$ hydrogenation path on Pd_{13} (path III in Scheme 1 and see Fig. 6). In the case of $Pd_{12}Ag$ and $Pd_{11}Ag_2$, there is only a slight difference in stability between $(CHCH_2 + H)^*$ and $(CH_2CH + H)^*$, and the G_a of $CHCH_2 + H$ is lower than that of $CH_2CH + H$ (32.72 *vs.* 145.32 kJ mol^{-1} for $Pd_{12}Ag$ and 4.29 *vs.* 77.33 kJ mol^{-1} for $Pd_{11}Ag_2$) (in Table 2). C_2H_2 hydrogenates in favor of path III on $Pd_{12}Ag$ and $Pd_{11}Ag_2$ too.

$Pd_{10}Ag_3$ prefers the $(CH_2CH + H)^*$ co-adsorption configuration and $CH_2CH + H$ hydrogenation path (I or II, 63.26 *vs.* 67.14 kJ mol^{-1} for $CHCH_2 + H$, Fig. S11†). Subsequently, there is only a slight difference between the desorption of CH_2CH_2 (ad) from $Pd_{10}Ag_3$ (104.48 kJ mol^{-1}) and further hydrogenation to C_2H_5 (101.28 kJ mol^{-1}). That is, both path I and path II can occur at the same time on $Pd_{10}Ag_3$, and the latter may be a priority.

For Pd_9Ag_4 and Pd_8Ag_5 clusters, the $(CHCH_2 + H)^*$ configuration is slightly more stable than the $(CH_2CH + H)^*$ configuration, so they may coexist on Pd_9Ag_4 and Pd_8Ag_5 (Fig. S12†). Path III is unlikely to occur because the barrier of $CHCH_3$ formation from the $C_2H_3 + H$ species on Pd_9Ag_4 (88.01 kJ mol^{-1}) is greater than that of CH_2CH_2 (ad) (61.21kJ mol^{-1}), but that on Pd_8Ag_5 is just the opposite (25.53 *vs.* 52.69 kJ mol^{-1}), preferring path III. Even if they form CH_2CH_2 (ad), they hydrogenate further to C_2H_5 instead of desorption on Pd_9Ag_4 (54.78 *vs.* 102.94 kJ mol^{-1}) and Pd_8Ag_5 (80.91 *vs.* 85.15 kJ mol^{-1}) (Table 2). The $CHCH_3$ hydrogenation path is dominant on Pd_7Ag_6, even though the larger barrier of $CHCH_3$ formation (125.25 kJ mol^{-1}) than CH_2CH_2 (ad) formation (59.62 kJ mol^{-1}) starting from $C_2H_3 + H$ species, as shown in Table 2 and Fig. S12†, $(CHCH_2 + H)^*$ is more stable. Even if CH_2CH_2 (ad) is formed, it prefers further hydrogenation to C_2H_5 rather than its desorption over Pd_7Ag_6 (44.96 *vs.* 84.27 kJ mol^{-1}).

When $(C_2H_3 + H)$ adsorbs on Pd_6Ag_7, the carbon atom bonded with two H atoms in C_2H_3 is suspended and far away from the cluster, and only the carbon atom bonded to one H atom is attached to the cluster, as shown in Fig. 6. The adsorption configuration of $(C_2H_3 + H)$ is only $(CH_2CH + H)^*$, that is, the $CHCH_3$ hydrogenation path (path III) is inhibited. For $Pd_{13-m}Ag_m$ ($8 \leq m \leq 10$), the adsorption configuration of $(C_2H_3 + H)$ is similar to that of Pd_6Ag_7 (except for Pd_5Ag_8, where the carbon atom bonded with one hydrogen atom in C_2H_3 is bridged with two Pd atoms of Pd_5Ag_8), and path III is inhibited on these clusters (see Fig. 6 and S11†). Then, it is just necessary to confirm whether CH_2CH_2 (ad) prefers desorption rather than its further hydrogenation on $Pd_{13-m}Ag_m$ ($7 \leq m \leq 10$). For Pd_6Ag_7, the G_a for the hydrogenation of CH_2CH_2 (ad) to C_2H_5 is 46.06 kJ mol^{-1}, compared with 23.18 kJ mol^{-1} for desorption. CH_2CH_2 (ad) preferentially desorbs from Pd_6Ag_7 rather than its further hydrogenation to C_2H_5. However, on Pd_5Ag_8, CH_2CH_2 (ad) is more likely to undergo further hydrogenation than desorption (49.16 *vs.* 74.98 kJ mol^{-1}, Fig. 6, S11† and Table 2), which can be interpreted as a stronger adsorption capacity of Pd_5Ag_8 to CH_2CH_2 (ad) (see Fig. 1 and Table 1). CH_2CH_2 (ad) preferentially desorbs from Pd_4Ag_9 rather than its further hydrogenation to C_2H_5 (60.59 *vs.* 80.65 kJ mol^{-1}). For Pd_3Ag_{10}, the hydrogenation of CH_2CH_2 (ad) to C_2H_5 is slightly advantageous over or competitive with desorption (52.85 *vs.* 59.31 kJ mol^{-1}, Table 2).

As presented in Table 2 and Fig. 6, the doping of Ag atoms also changes the progress of acetylene hydrogenation, that is, the RDS (with larger G_a) of two-step hydrogenation is transferred. Ag atoms cause the evolution of bimetallic cluster structures, which tunes the catalytic performance for acetylene semi-hydrogenation. Pd_6Ag_7 and Pd_4Ag_9 are favorable for acetylene hydrogenation to CH_2CH_2 (ad), and subsequently desorption from the catalyst rather than further hydrogenation (path I).

Effect of Ag doping on the activity and selectivity of CH_2CH_2 formation

The catalytic activity of the corresponding $Pd_{13-m}Ag_m$ clusters toward the formation of CH_2CH_2 is estimated from the reaction rate calculated through a two-step model according to the following eqn (5), which has been systematically reported by Hu *et al.* and others.[48–51]

$$r = \frac{k_B T}{h} \frac{1 - \frac{P_P}{P_R} e^{\frac{\Delta G}{RT}}}{\frac{P^0}{P_R} e^{\frac{G_R^{ad} - G_R^{de} + G_P^{de}}{RT}} + e^{\frac{G_P^{de}}{RT}}} \quad (5)$$

where k_B, T, h, R are the Boltzmann constant, temperature, Planck constant and universal gas constant, respectively; P_R and P_P represent the partial pressure of the reactant and product, respectively and ΔG, G_R^{ad}, G_R^{de} and G_P^{de} are the reaction free energy of C_2H_2 hydrogenation to CH_2CH_2, and the effective free barriers of reactant adsorption, reactant desorption and product desorption, respectively. With the purpose of reflecting the catalytic performance of the clusters under real reaction conditions, the relevant parameters in the calculations of the reaction rate are selected as follows: the ratio of H_2 and C_2H_2 is 10, and the CH_2CH_2, C_2H_2 and H_2 species correspond to the partial pressures of 0.89, 0.01 and 0.1 atm, respectively. Thus, P_R and P_P are 0.11 and 0.89 atm, respectively.

The reaction rates for the hydrogenation of acetylene to ethylene on $Pd_{13-m}Ag_m$ clusters calculated using eqn (5) are shown in Table 2. The reaction rate of acetylene hydrogenation to ethylene on Pd_6Ag_7 is 1.25×10^{10} per s site, compared with 3.13×10^5 per s site on Pd_4Ag_9. Pd_{13}, $Pd_{11}Ag_2$, Pd_9Ag_4, Pd_7Ag_6 and Pd_5Ag_8 still exhibit poor CH_2CH_2 selectivity, which is shown in the results of Table 2.[52] The selectivity of CH_2CH_2 is 4.43, −3.20, −4.24 and −6.46 kJ mol^{-1} on $Pd_{12}Ag$, $Pd_{10}Ag_3$, Pd_8Ag_5 and Pd_3Ag_{10}, respectively, indicating that further hydrogenation of CH_2CH_2 is competitive with desorption. For Pd_6Ag_7 and Pd_4Ag_9, the selectivity of CH_2CH_2 is 22.88 and 20.06 kJ mol^{-1}, respectively. However, the adsorption free energy of CH_2CH_2 on Pd_6Ag_7 (co-adsorption with the H atom) is only −23.18 kJ mol^{-1}, desorption of which is easy. This shows that Pd_6Ag_7 is more conducive to the semi-hydrogenation of acetylene to ethylene.

The most stable cluster may not necessarily exhibit the best catalytic performance; instead clusters with unique electronic structures and accessible low-energy metastable structures may contribute to the excellent adsorption/transformation of reactants.[53,54] The structural properties of $Pd_{13-m}Ag_m$ clusters, which are central to comprehending their catalytic performance for acetylene semi-hydrogenation, have been studied in detail in our previous work.[29] With the variation of Ag atom content in $Pd_{13-m}Ag_m$ clusters, the metal–metal interaction in the clusters has changed, affecting the stability of clusters. Regardless of the perspective of energy or electrons, Pd_5Ag_8 has the most stable composition among the 13-atom bimetallic clusters. As discussed above, however, the catalytic performance of Pd_5Ag_8 for acetylene semi-hydrogenation is not good. Opposition between stability and catalytic activity is often encountered in research on catalysis, namely, the stability of catalysts is not always positively correlated with their reactivity. Sure enough, the low-energy metastable composition of Pd_6Ag_7 exhibits the best activity and selectivity for ethylene formation. The unique distribution of palladium and silver in Pd_6Ag_7 promotes the adsorption and activation of acetylene and the desorption of ethylene, which is more conducive to the semi-hydrogenation of acetylene to ethylene under the reaction conditions. The most stable composition for the $Pd_{13-m}Ag_m$ clusters is Pd_5Ag_8 associated with stronger interaction between ethylene molecules, and hence shows poor ethylene selectivity. The most stable bimetallic cluster is not the best composition for acetylene semi-hydrogenation. Instead, the metastable bimetallic cluster with diverse compositions contributes to the high activities and selectivity for ethylene formation.

4. Conclusions

We explore the effect of a dizzying variety of Ag-induced structural and electronic properties of $Pd_{13-m}Ag_m$ clusters on their catalytic performance of acetylene semi-hydrogenation by computation chemistry. The adsorption configurations of acetylene and ethylene on a series of bimetallic clusters are identified, which are closely related to the structural evolution induced by Ag. With an increase in the content of Ag, a transformation of acetylene adsorption configurations from a tetra-σ mode (Pd_{13}~$Pd_{11}Ag_2$) to a di-σ/π mode ($Pd_{10}Ag_3$~Pd_6Ag_7), then to a di-σ mode (Pd_5Ag_8) and finally to a π mode (Pd_4Ag_9~Ag_{13}) was observed. However, ethylene has only two adsorption modes, di-σ (Pd_{13}~Pd_7Ag_6) and π mode (Pd_6Ag_7~Ag_{13}). Electronic structural analysis reveals that the adsorption configuration is governed by the HOMO structures of the clusters dominated by intra-cluster metal–metal interactions.

Acetylene hydrogenation on $Pd_{13-m}Ag_m$ clusters was systematically investigated. The doping of Ag atoms can effectively tune the hydrogenation path of acetylene, and the RDS of the reaction is also transferred. Excessive hydrogenation of acetylene could not be prevented by too much or too little Ag doping. The activity and selectivity of acetylene semi-hydrogenation on the Pd_5Ag_8 cluster, which is the most stable composition, are not good. Instead, the low-energy metastable Pd_6Ag_7 exhibits optimal ethylene formation activity and selectivity, attributed to its unique geometric and electronic structure,

which can effectively activate acetylene and weaken the adsorption strength of ethylene. The proposed mechanism is generally applicable, providing an interesting opportunity for the design and development of novel sub-nanometric bimetallic catalysts.

Author contributions

Panpeng Wei: conceptualization, methodology, investigation, writing – original draft, and writing – review and editing. Jian Zheng and Qing Li: methodology and software. Yucai Qin: writing – review and editing. Huimin Guan and Duping Tan: writing – review and editing. Lijuan Song: methodology, software, supervision, project administration, and funding acquisition.

Conflicts of interest

There are no conflicts to declare.

Acknowledgements

This work was supported by the National Natural Science Foundation of China (U1908203) and the Natural Science Foundation of Liaoning Province (2020-MS-284).

Notes and references

1 J. L. Carter, G. B. McVinker, W. Weissman, M. S. Kmak and J. H. Sinfelt, Bimetallic catalysts; Application in catalytic reforming, *Appl. Catal.*, 1982, **3**, 327–346.
2 M. Sankar, N. Dimitratos, P. J. Miedziak, P. P. Wells, C. J. Kiely and G. J. Hutchings, Designing bimetallic catalysts for a green and sustainable future, *Chem. Soc. Rev.*, 2012, **41**, 8099–8139.
3 Z. Wei, J. Sun, Y. Li, A. K. Datye and Y. Wang, Bimetallic catalysts for hydrogen generation, *Chem. Soc. Rev.*, 2012, **41**, 7994–8008.
4 H. Rong, S. Ji, J. Zhang, D. Wang and Y. Li, Synthetic strategies of supported atomic clusters for heterogeneous catalysis, *Nat. Commun.*, 2020, **11**, 5884.
5 B. Coq and F. Figueras, Bimetallic palladium catalysts: influence of the co-metal on the catalyst performance, *J. Mol. Catal. A: Chem.*, 2001, **173**, 117–134.
6 C. Yang, B. H. Ko, S. Hwang, Z. Liu, Y. Yao, W. Luc, M. Cui, A. S. Malkani, T. Li, X. Wang, J. Dai, B. Xu, G. Wang, D. Su, F. Jiao and L. Hu, Overcoming immiscibility toward bimetallic catalyst library, *Sci. Adv.*, 2020, **6**, eaaz6844.
7 M. Kuhn, M. Lucas and P. Claus, Long-time stability vs deactivation of Pd–Ag/Al_2O_3 egg-shell catalysts in selective hydrogenation of acetylene, *Ind. Eng. Chem. Res.*, 2015, **54**, 6683–6691.
8 A. Borodziński and G. C. Bond, Selective hydrogenation of ethyne in ethene-rich streams on palladium catalysts. Part 1. Effect of changes to the catalyst during reaction, *Catal. Rev.*, 2006, **48**, 91–144.
9 F. Studt, F. Abild-Pedersen, T. Bligaard, R. Z. Sorensen, C. H. Christensen and J. K. Norskov, On the role of surface modifications of palladium catalysts in the selective hydrogenation of acetylene, *Angew. Chem., Int. Ed.*, 2008, **47**, 9299–9302.
10 F. Studt, F. Abild-Pedersen, T. Bligaard, R. Z. Sorensen, C. H. Christensen and J. K. Norskov, Identification of non-precious metal alloy catalysts for selective hydrogenation of acetylene, *Science*, 2008, **320**, 1320–1322.
11 Q. Li, Y. Qin, D. Tan, Y. Xie, M. Lv and L. Song, Theoretical investigation of conversion between different C_2H_x species over Pd–Ag/Pd(100) surface alloys: influence on the selectivity and transformation of carbonaceous species, *New J. Chem.*, 2018, **42**, 19827–19836.
12 F. Liu, Y. Xia, W. Xu, L. Cao, Q. Guan, Q. Gu, B. Yang and J. Lu, Integration of bimetallic electronic synergy with oxide site isolation improves the selective hydrogenation of acetylene, *Angew. Chem., Int. Ed.*, 2021, **60**, 19324–19330.
13 K. Kokko, R. Laihia, M. Alatalo, P. T. Salo, M. P. J. Punkkinen, I. J. Väyrynen, W. Hergert and D. Ködderitzsch, From X-ray-absorption near-edge structures to the d-hole population in Pd–Ag alloys, *Phys. Rev. B: Condens. Matter Mater. Phys.*, 1999, **60**, 4659–4664.
14 H. Zhou, X. Yang, L. Li, X. Liu, Y. Huang, X. Pan, A. Wang, J. Li and T. Zhang, PdZn intermetallic nanostructure with Pd–Zn–Pd ensembles for highly active and chemoselective semi-hydrogenation of acetylene, *ACS Catal.*, 2016, **6**, 1054–1061.
15 G. Kyriakou, M. B. Boucher, A. D. Jewell, E. A. Lewis, T. J. Lawton, A. E. Baber, H. L. Tierney, M. Flytzani-Stephanopoulos and E. C. H. Sykes, Isolated metal atom geometries as a strategy for selective heterogeneous hydrogenations, *Science*, 2012, **335**, 1209–1212.
16 X. T. Li, L. Chen, C. Shang and Z. P. Liu, In situ surface structures of PdAg catalyst and their influence on acetylene semihydrogenation revealed by machine learning and experiment, *J. Am. Chem. Soc.*, 2021, **143**, 6281–6292.
17 D. Teschner, J. Borsodi, A. Wootsch, Z. Révay, M. Hävecker, A. Knop-Gericke, S. D. Jackson and R. Schlögl, The roles of subsurface carbon and hydrogen in palladium-catalyzed alkyne hydrogenation, *Science*, 2008, **320**, 86–89.
18 T. Mitsudome, T. Urayama, K. Yamazaki, Y. Maehara, J. Yamasaki, K. Gohara, Z. Maeno, T. Mizugaki, K. Jitsukawa and K. Kaneda, Design of core-Pd/shell-Ag nanocomposite catalyst for selective semihydrogenation of alkynes, *ACS Catal.*, 2015, **6**, 666–670.
19 G. X. Pei, X. Y. Liu, A. Wang, A. F. Lee, M. A. Isaacs, L. Li, X. Pan, X. Yang, X. Wang, Z. Tai, K. Wilson and T. Zhang, Ag alloyed Pd single-atom catalysts for efficient selective hydrogenation of acetylene to ethylene in excess ethylene, *ACS Catal.*, 2015, **5**, 3717–3725.

20 Q. Li, Y. Ma, H. Qi, Z. Mo, X. Zhang and L. Song, Impact of surface arrangement and composition on ethylene adsorption over Pd–Ag surface alloys: a computational study, *RSC Adv.*, 2016, **6**, 70932–70942.
21 S. González, K. M. Neyman, S. Shaikhutdinov, H. J. Freund and F. Illas, On the promoting role of Ag in selective hydrogenation reactions over Pd–Ag bimetallic catalysts: A theoretical study, *J. Phys. Chem. C*, 2007, **18**, 6852–6856.
22 Q. Li, L. Song, L. Pan, X. Zhuang, M. Ling and L. Duan, Ensemble and ligand effects on the acetylene adsorption on ordered Pd_xAg_{1-x}/Pd(100) surface alloys investigated by periodic DFT study, *Phys. Chem. Chem. Phys.*, 2013, **15**, 20345–20353.
23 A. A. Herzing, C. J. Kiely, A. F. Carley, P. Landon and G. J. Hutchings, Identification of active gold nanoclusters on iron oxide supports for CO oxidation, *Science*, 2008, **321**, 1331–1335.
24 C. Dong, Y. Li, D. Cheng, M. Zhang, J. Liu, Y.-G. Wang, D. Xiao and D. Ma, Supported metal clusters: Fabrication and application in heterogeneous catalysis, *ACS Catal.*, 2020, **10**, 11011–11045.
25 R. Li, X. Xu, B. Zhu, X.-Y. Li, Y. Ning, R. Mu, P. Du, M. Li, H. Wang, J. Liang, Y. Chen, Y. Gao, B. Yang, Q. Fu and X. Bao, In situ identification of the metallic state of Ag nanoclusters in oxidative dispersion, *Nat. Commun.*, 2021, **12**, 1406.
26 C. Dong, Z. Gao, Y. Li, M. Peng, M. Wang, Y. Xu, C. Li, M. Xu, Y. Deng, X. Qin, F. Huang, X. Wei, Y.-G. Wang, H. Liu, W. Zhou and D. Ma, Fully exposed palladium cluster catalysts enable hydrogen production from nitrogen heterocycles, *Nat. Catal.*, 2022, 1–9.
27 X. Liu, G. Saranya, X. Huang, X. Cheng, R. Wang, M. Chen, C. Zhang, T. Li and Y. Zhu, $Ag_2Au_{50}(PET)_{36}$ nanocluster: Dimeric assembly of $Au_{25}(PET)_{18}$ enabled by silver atoms, *Angew. Chem., Int. Ed.*, 2020, **59**, 13941–13946.
28 N. A. Khan, A. Uhl, S. Shaikhutdinov and H. J. Freund, Alumina supported model Pd–Ag catalysts: A combined STM, XPS, TPD and IRAS study, *Surf. Sci.*, 2006, **600**, 1849–1853.
29 P. Wei, J. Zheng, Q. Li, Y. Qin and L. Song, The role of silver in 13-atom palladium–silver bimetallic clusters: Nucleation and growth, structural evolution, electron interaction, *J. Mater. Sci.*, 2022, **57**, 8180–8194.
30 M. Heemeier, A. F. Carlsson, M. Naschitzki, M. Schmal, M. Bäumer and H. J. Freund, Preparation and characterization of a model bimetallic catalyst: Co–Pd nanoparticles supported on Al_2O_3, *Angew. Chem., Int. Ed.*, 2002, **41**, 4073–4076.
31 M. Crespo-Quesada, F. Cárdenas-Lizana, A.-L. Dessimoz and L. Kiwi-Minsker, Modern trends in catalyst and process design for alkyne hydrogenations, *ACS Catal.*, 2012, **2**, 1773–1786.
32 D. Liu, DFT study of selective hydrogenation of acetylene to ethylene on Pd doping Ag nanoclusters, *Appl. Surf. Sci.*, 2016, **386**, 125–137.
33 H.-Y. Ma and G.-C. Wang, Selective hydrogenation of acetylene on Pt_n/TiO_2 (n=1, 2, 4, 8) surfaces: Structure sensitivity analysis, *ACS Catal.*, 2020, **10**, 4922–4928.
34 J. Zhang, M. Wang, Z. Gao, X. Qin, Y. Xu, Z. Wang, W. Zhou and D. Ma, Importance of species heterogeneity in supported metal catalysts, *J. Am. Chem. Soc.*, 2022, **11**, 5108–5115.
35 I. Karakaya and W. T. Thompson, The Ag–Pd (silver–palladium) system, *Bull. Alloy Phase Diagrams*, 1988, **9**, 237–243.
36 S. J. Clark, M. D. Segall, C. J. Pickard, P. J. Hasnip, M. I. Probert, K. Refson and M. C. Payne, First principles methods using CASTEP, *Z. Kristallogr.*, 2005, **220**, 567–570.
37 J. P. Perdew and Y. Wang, Accurate and simple analytic representation of the electron–gas correlation energy, *Phys. Rev. B: Condens. Matter Mater. Phys.*, 1992, **45**, 13244.
38 F. Abild-Pedersen, J. Greeley and J. K. Nørskov, Understanding the effect of steps, strain, poisons, and alloying: Methane activation on Ni surfaces, *Catal. Lett.*, 2005, **105**, 9–13.
39 Q. Li, L. Song, L. Pan, Y. Chen, M. Ling, X. Zhuang and X. Zhang, Density functional theory studies of electronic properties of PdAg/Pd surface alloys, *Appl. Surf. Sci.*, 2014, **288**, 69–75.
40 S. Kirkpatrick, C. D. Gelatt Jr. and M. P. Vecchi, Optimization by simulated annealing, *Science*, 1983, **220**, 671–680.
41 R. Sowdhamini, D. F. Burke, J. F. Huang, K. Mizuguchi, H. A. Nagarajaram, N. Srinivasan, R. E. Steward and T. L. Blundell, CAMPASS: A database of structurally aligned protein superfamilies, *Structure*, 1998, **6**, 1087–1094.
42 P. Timbrell, A. Gellman, R. Lambert and R. Willis, Negative ion resonance selective mode enhancement in the hreel spectrum of C_2H_2 on Pd (111), *Surf. Sci.*, 1988, **206**, 339–347.
43 J. C. Dunphy, M. Rose, S. Behler, D. F. Ogletree, M. Salmeron and P. Sautet, Acetylene structure and dynamics on Pd (111), *Phys. Rev. B*, 1998, **57**, 12705–12708.
44 X.-R. Shi, S.-G. Wang and J. Wang, Chemisorption of oxygen and subsequent reactions on low index surfaces of β-Mo_2C: Insights from first-principles thermodynamics and kinetics, *J. Mol. Catal. A: Chem.*, 2016, **417**, 53–63.
45 F. Abild-Pedersen, J. Greeley, F. Studt, J. Rossmeisl, T. R. Munter, P. G. Moses, E. Skulason, T. Bligaard and J. K. Norskov, Scaling properties of adsorption energies for hydrogen-containing molecules on transition-metal surfaces, *Phys. Rev. Lett.*, 2007, **99**, 016105.
46 B. Hammer and J. K. Norskov, Why gold is the noblest of all the metals, *Nature*, 1995, **376**, 238–240.
47 J.-N. Li, M. Pu, C.-C. Ma, Y. Tian, J. He and D. G. Evans, The effect of palladium clusters (Pd_n, n=2–8) on mechanisms of acetylene hydrogenation: A DFT study, *J. Mol. Catal. A: Chem.*, 2012, **359**, 14–20.
48 J. Cheng, P. Hu, P. Ellis, S. French, G. Kelly and C. M. Lok, Brønsted–Evans–Polanyi relation of multistep reactions and volcano curve in heterogeneous catalysis, *J. Phys. Chem. C*, 2008, **112**, 1308–1311.
49 J. Cheng and P. Hu, Theory of the kinetics of chemical potentials in heterogeneous catalysis, *Angew. Chem., Int. Ed.*, 2011, **50**, 7650–7654.

50 R. Zhang, J. Zhang, Z. Jiang, B. Wang and M. Fan, The cost-effective Cu-based catalysts for the efficient removal of acetylene from ethylene: The effects of Cu valence state, surface structure and surface alloying on the selectivity and activity, *Chem. Eng. J.*, 2018, **351**, 732–746.
51 B. Yang, R. Burch, C. Hardacre, G. Headdock and P. Hu, Influence of surface structures, subsurface carbon and hydrogen, and surface alloying on the activity and selectivity of acetylene hydrogenation on Pd surfaces: A density functional theory study, *J. Catal.*, 2013, **305**, 264–276.
52 L. Xu, E. E. Stangland and M. Mavrikakis, Ethylene versus ethane: A DFT-based selectivity descriptor for efficient catalyst screening, *J. Catal.*, 2018, **362**, 18–24.
53 Z. Zhang, B. Zandkarimi and A. N. Alexandrova, Ensembles of metastable states govern heterogeneous catalysis on dynamic interfaces, *Acc. Chem. Res.*, 2020, **53**, 447–458.
54 G. Sun and P. Sautet, Metastable structures in cluster catalysis from first-principles: Structural ensemble in reaction conditions and metastability triggered reactivity, *J. Am. Chem. Soc.*, 2018, **140**, 2812–2820.